Least-squares interband denoising of color and multispectral images

P. Scheunders, J. Driesen
Vision Lab, Department of Physics, University of Antwerp
Groenenborgerlaan 171, 2020 Antwerpen, Belgium
Tel.: +32 3 218 04 39; Fax.: +32 3 218 03 18
Email: scheun@ruca.ua.ac.be, Jef.Driesen@ua.ac.be

Abstract

This paper exploits the interband correlations of color and multispectral images for wavelet-based denoising. For this, a multispectral extension of the linear minimum mean squared error estimation (LMMSE) is constructed to estimate the signal from the observed wavelet coefficients. The calculation involves the signal autocovariance matrices, which are estimated globally or locally for centered square windows using Maximum Likelihood and MAP. The method is demonstrated to outperform single-band denoising on color and 7-band Landsat multispectral images.

1 Introduction

With the evolution of imaging technology, an increasing number of imaging modalities becomes available. In remote sensing, sensors are available that can generate multispectral data. In multispectral imagery, noise handling may be important. Due to physical constraints, a trade-off exists between spatial and spectral resolution and SNR. Also, noise filtering and image enhancement can drastically facilitate the processing and analysis of multispectral imagery.

The paradigm of wavelet denoising originates from [1]. There, a threshold value was derived using the discrete wavelet transform [2]. The threshold value was *universal*, i.e. independent of the subband, and *soft*, i.e. all wavelet coefficients below the threshold were removed, and all others were shrunk by the threshold value. Later on, threshold values were derived that became adaptive, i.e. dependent of the specific subband. For this, Bayesian approaches were applied, where a prior for the signal pdf was assumed (see e.g. [3] and references therein). Also spatially adaptive thresholds were derived [4]. Further on, it was suggested that shift-invariant versions of the wavelet transform were favored over the discrete wavelet transform. This was also suggested in [5].

Another approach estimates the true signal by a linear minimal mean squared error (LMMSE) technique instead of thresholding. In [6], this technique was applied by Maximum A Posteriori (MAP) estimation of the (spatially local) signal variance, imposing some prior on it. In [7], the interscale correlations were exploited using a vector-valued LMMSE approach. In this work, the latter idea is applied to exploit the high correlation that typically exists between different bands for improving the denoising of color and multispectral images.

2 Multivalued image LMMSE denoising

Suppose an N-band multivalued image $\mathbf{I}(x,y) = (I_1(x,y), I_2(x,y), ..., I_N(x,y))^T$. The additive image noise is modelled as a Gaussian random vector with independent components of equal variance. For $i = 1, \cdots, N$:

$$I_i(x,y) = s_i(x,y) + n_i(x,y)$$
$$f_x(x = n_i) = g_x(0, \sigma^2) = \frac{1}{\sqrt{2\pi}\sigma} \exp\left(\frac{-x^2}{2\sigma^2}\right) \quad (1)$$

As mentioned before, redundant wavelet-transforms are favored over orthogonal ones, because of their shift-invariance property. The applied wavelet transform in this paper is the redundant dyadic transform from Mallat [8]. For this transform, the mother wavelets $\psi^x(x,y)$ and $\psi^y(x,y)$ are quadratic spline wavelets of compact support. The detail images $D_i^{(j)*}(x,y)$ are convolutions in the $*$-direction ($* = x$ or y) of each band i with scaled versions of these mother wavelets; the scale parameter j is a power of 2.

After wavelet transformation, the noise of the detail images (we will omit $*$) will be Gaussian [5]:

$$D_i^{(j)}(x,y) = S_i^{(j)}(x,y) + N_i^{(j)}(x,y)$$
$$f_x(x = N_i^{(j)}) = g_x(0, \sigma_n^{(j)2}) \qquad \sigma_n^{(j)} = \|\psi_j\|\sigma \quad (2)$$

0-7803-8554-3/04/$20.00 ©2004 IEEE.

2.1 single band LMMSE

The linear minimum mean squared error (LMMSE) estimate of the signal coefficient $S_i^{(j)}$ of band i at scale j is given by (from here, we will omit (j), since the expressions are identical for different scales):

$$\hat{S}_i = \frac{\sigma^2(S_i)}{\sigma^2(S_i) + \sigma_n^2} D_i \tag{3}$$

where $\sigma^2(S_i)$ is the signal variance. The latter can be estimated in different ways. On the global image (of size $M \times N$):

$$\hat{\sigma}_G^2(S_i) = \frac{1}{MN} \sum_{m,n=1}^{M,N} D_i^2(m,n) - \sigma_n^2 \tag{4}$$

In [6], a block-based estimation, using maximum-likelihood is proposed:

$$\hat{\sigma}_{ML}^2(S_i) = \max\left(0, \sigma_B^2(D_i) - \sigma_n^2\right) \tag{5}$$

with $\sigma_B^2(D_i) = \frac{1}{N_\Lambda} \sum_{(m,n)\in\Lambda} D_i^2(m,n)$, where Λ is a centered square block, with N_Λ points. In the same work, a MAP estimator is proposed, imposing an exponential prior on $\sigma^2(S_i)$, $f(\sigma^2(S_i)) = \lambda \exp\{-\lambda\sigma^2(S_i)\}$, leading to:

$$\hat{\sigma}_{MAP}^2(S_i) = \max\left(0, \frac{N_\Lambda}{4\lambda} \left[-1 + \sqrt{1 + \frac{8\lambda}{N_\Lambda}\sigma_B^2(D_i)}\right] - \sigma_n^2\right) \tag{6}$$

with λ, the parameter from the exponential prior. λ can e.g. be estimated as $1/ < \hat{\sigma}_{ML}^2(S_i) >$.

2.2 interband LMMSE

Estimators 4, 5 and 6 are based on the LMMSE estimation of each band separately. A vector-valued LMMSE estimator can be obtained for $\mathbf{D} = (D_1, ..., D_N)^T$. For this vector:

$$\mathbf{D} = \mathbf{S} + \mathbf{N} \tag{7}$$

with $\mathbf{S} = (S_1, ..., S_N)^T$ and $\mathbf{N} = (N_1, ..., N_N)^T$, the latter denoting Gaussian independent vector noise. The LMMSE estimate of $\mathbf{S}$ can be computed as:

$$\hat{\mathbf{S}} = \Sigma(\Sigma + R)^{-1}\mathbf{D} \tag{8}$$

where Σ and R are the covariance matrices of $\mathbf{S}$ and $\mathbf{N}$, respectively:

$$\Sigma = E[\mathbf{S}\mathbf{S}^T] = E\begin{bmatrix} S_1^2 & \cdots & S_1 S_N \\ \vdots & \ddots & \vdots \\ S_N S_1 & \cdots & S_N^2 \end{bmatrix} \tag{9}$$

and

$$R = E[\mathbf{N}\mathbf{N}^T] = E\begin{bmatrix} \sigma_n^2 & \cdots & 0 \\ \vdots & \ddots & \vdots \\ 0 & \cdots & \sigma_n^2 \end{bmatrix} \tag{10}$$

The latter being diagonal since the noise between bands is supposed to be uncorrelated.

Estimation of the signal covariance elements can be done in similar ways as for the single-band case. On the global image:

$$\hat{\Sigma}_G(i,k) = E[S_i S_k] = \frac{1}{MN} \sum_{m,n=1}^{M,N} (D_i \cdot D_k)(m,n) - \delta_{i,k}\sigma_n^2 \tag{11}$$

Locally adaptive, on a centered square block Λ:

$$\hat{\Sigma}_{ML}(i,k) = \max\left(0, \Sigma_B(D_{ik}) - \delta_{i,k}\sigma_n^2\right) \tag{12}$$

where

$$\Sigma_B(D_{ik}) = \frac{1}{N_\Lambda} \sum_{(m,n)\in\Lambda} (D_i \cdot D_k)(m,n) \tag{13}$$

Finally, an exponential prior can be imposed on $\Sigma(i,k)$: $f(\Sigma(i,k)) = \lambda_{i,k} \exp\{-\lambda_{i,k}\Sigma(i,k)\}$. The MAP estimator is then given as:

$$\hat{\Sigma}_{MAP}(i,k) = \max\left(0, \frac{N_\Lambda}{4\lambda_{i,k}} \left[-1 + \sqrt{1 + \frac{8\lambda_{i,k}}{N_\Lambda}\Sigma_B(D_{ik})}\right] - \delta_{i,k}\sigma_n^2\right) \tag{14}$$

$\lambda_{i,k}$ can e.g. be estimated as $1/ < \hat{\Sigma}_{ML}(i,k) >$.

Estimators 11, 12 and 14 take into account the interband correlations of the signal, and therefore are expected to outperform the single band estimators. In the next section, this will be evaluated for color and multispectral images.

3 Experiments and discussion

In this section, the interband LMMSE technique is evaluated and compared to single band LMMSE for an RGB color image LENA and a 7-band Landsat multispectral image. In figure 1, a zoomed part of the original color image and a version with added noise with $\sigma = 20$ is shown. Each time, the three estimators for the signal: on the global image, locally using ML and locally using MAP, that were described in the previous section, are applied. In total, 6 different techniques are compared and referred to as: SGL, SML, SMAP for single band LMMSE, and MGL, MML and MMAP for interband LMMSE.

σ	SGL	SML	SMAP	MGL	MML	MMAP
10	31.70	33.60	33.31	32.72	34.06	33.71
15	30.07	31.75	31.53	31.12	32.10	31.54
20	29.01	30.45	30.33	30.05	30.69	30.45
10	28.81	29.38	29.29	30.16	30.08	30.06
15	25.91	26.61	26.47	27.65	27.38	27.29
20	24.12	24.81	24.64	25.98	25.68	25.37

Table 1. PSNR values for the denoised color (first 3 rows) and multispectral image (last 3 rows) using the 6 different estimators

On each band of the image, gaussian noise with standard deviation σ was added. Each band is then wavelet transformed using the dyadic wavelet frames, up to 4 scales. For each scale, and each direction x and y, the estimator is applied. For the local estimators, a window size of 7×7 is applied.

In Table 1, PSNR values are shown for three different values of σ. In figure 2, zoomed denoised images are shown for the color image, using SGL, SML, MGL and MML respectively. From the table and from visual inspection of the denoised images, we derived the following conclusions:

- In all cases, the multiband estimators outperformed their single band counterparts. This holds for the global as well as for the local estimators. Visual inspection of the denoised images reveals an overall improved denoising performance while details are better preserved.

- On the color image, local estimators outperform the global estimator. On the Landsat image, this is not the case for multiband estimation. In fact, the method failed when higher scales than the first were taken into account (therefore, only the first scale was taken into account for the the PSNR values that are given in the table). This is caused by the fact that the multispectral image is highly textured. The assumption that pixels in a local region contain the same statistics, is not valid in such cases. Moreover, the correlation between textures of different bands is low, so that the multiband approach is not expected to lead to large improvements

- In all cases the Maximum Likelihood estimator outperforms the MAP estimator in PSNR values. This is somewhat surprising, since the MAP estimator was demonstrated to be an improved estimator of the signal standard deviation [6]. Visual inspection of the denoised results indeed reveals annoying local artifacts using ML. Using MAP, these artifacts disappear but the image becomes oversmoothed.

Based on these observations, we designed an improved estimator using a heuristic argument. The visual artifacts seem to be high-frequency effects that are mostly caused by local denoising at the highest wavelet scale. These can be removed by performing global denoising on the highest scale. Denoising on the other scales is done locally. Using this heuristic rule, we observed that the obtained PSNR values of the local MML estimator remains more or less the same, while the visual artifacts disappear almost completely. Details are better preserved than with the MAP estimator.

References

[1] D.L. Donoho and I.M. Johnstone, "Ideal spatial adaptation via wavelet shrinkage," *Biometrika*, vol. 81, pp. 425–455, 1994.

[2] S. Mallat, "A theory for multiresolution signal decomposition : the wavelet representation," *IEEE Transactions on Pattern Analysis and Machine Intelligence*, vol. 11, no. 7, pp. 674–693, 1989.

[3] S. Grace Chang, B. Yu, and M. Vetterli, "Adaptive wavelet thresholding for image denoising and compression," *IEEE Transactions on Image Processing*, vol. 9:(9), pp. 1532–1546, 2000.

[4] S. Grace Chang, B. Yu, and M. Vetterli, "Spatially adaptive wavelet thresholding with context modeling for image denoising," *IEEE Transactions on Image Processing*, vol. 9:(9), pp. 1522–1531, 2000.

[5] Q. Pan, L. Zhang, and G. Dai aand H. Zhang, "Two denoising methods by wavelet transform," *IEEE Transactions on Signal Processing*, vol. 47:(12), pp. 3401–3406, 1999.

[6] M.K. Mihcak, I. Kozintsev, K. Ramachandran, and P. Moulin, "Low-complexity image denoising based on statistical modeling of wavelet coefficients," *IEEE Signal Processing Letters*, vol. 6:(12), pp. 300–303, 1999.

[7] L. Zhang, P.Bao, and X. Wu, "Hybrid inter- and intra-wavelet scale image restoration," *Pattern Recognition*, vol. 36:(8), pp. 1737–1746, 2003.

[8] S. Mallat and S. Zhong, "Characterization of signals from multiscale edges," *IEEE Trans. Pattern Anal. Machine Intell.*, vol. 14, pp. 710–732, 1992.

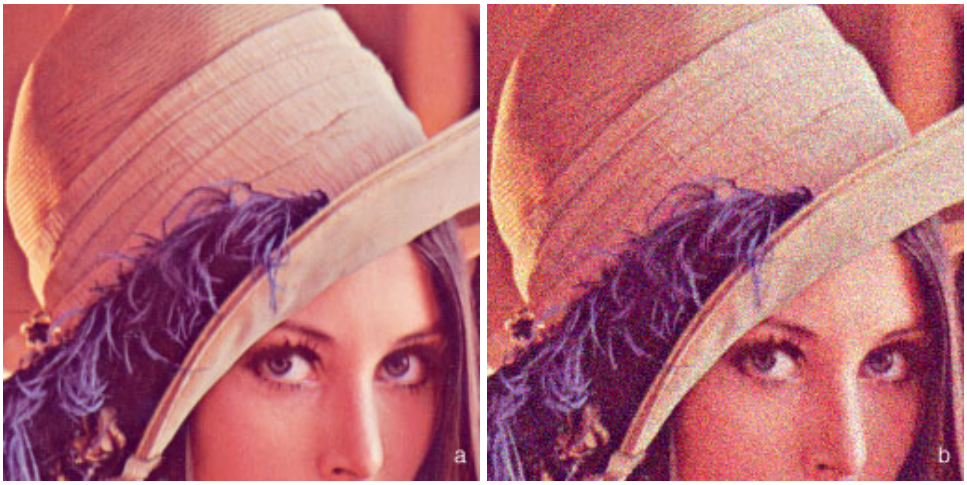

Figure 1. Zoomed image Lena; a: original; b: noisy image with $\sigma = 20$

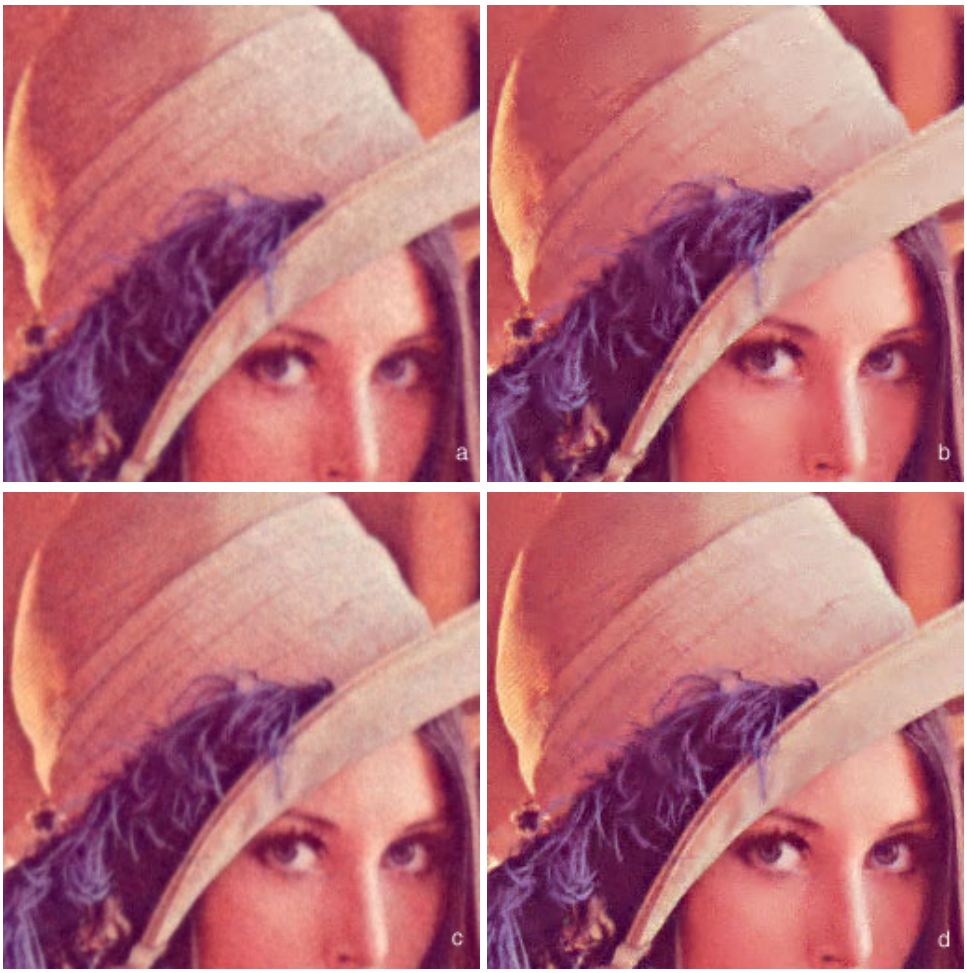

Figure 2. Zoomed denoised image Lena, using a: SGL (PSNR=29.01); b: SML (PSNR=30.45); c: MGL (PSNR=30.05) and d: MML (PSNR=30.69)